

Energy-loss calculation of swift C_n^+ ($n=2-60$) clusters through thin foils

Santiago Heredia-Avalos and Rafael Garcia-Molina

Departamento de Física — CIOyN, Universidad de Murcia, Apartado 4021, E-30080 Murcia, Spain

Isabel Abril

Departament de Física Aplicada, Universitat d'Alacant, Apartat 99, E-03080 Alacant, Spain

(Received 4 May 2006; revised manuscript received 30 March 2007; published 23 July 2007)

The energy loss of swift C_n^+ ($n=2-60$) clusters moving with velocity $1 \leq v \leq 4$ a.u. ($0.3 \leq E \leq 6$ MeV/atom) through carbon, aluminum, and silicon thin foils has been calculated. We have considered that the carbon atomic ions resulting from the dissociation of these clusters feel Coulomb explosion, stopping, and wake forces due to the target polarization, as well as nuclear scattering with the target nuclei; the three former interactions depend on the ion charge state, which can change during its travel through the foil, due to electron-capture and -loss processes. Our calculation predicts an enhancement of the average energy loss of each dissociated atomic ion in comparison with the case of the same, but isolated, carbon atomic ion, which is small for velocities $v \sim 1$ a.u. and becomes more important for higher velocities ($v \sim 4$ a.u.). The energy loss of the dissociated atomic ions generally increases with the size and packing level of the cluster, although in some cases it tends to a saturation value (when the number of constituents of the cluster increases) or it could even decrease with cluster size for certain situations (for projectiles with $1 \leq v \leq 2$ a.u. in aluminum or silicon targets). The vicinage effects in the energy loss also depend on the target nature, being more important for silicon and aluminum foils than for amorphous carbon foils. Our results show that in most cases the highest enhancement in energy loss should be expected for large clusters with high projectile velocities in aluminum or silicon targets. The experimental energy loss measured in carbon targets is well reproduced by our calculations.

DOI: [10.1103/PhysRevA.76.012901](https://doi.org/10.1103/PhysRevA.76.012901)

PACS number(s): 34.50.Bw, 36.40.-c, 61.48.+c

I. INTRODUCTION

The study of the differences between the energy loss of a single atomic ion or an ensemble of atomic ions is an interesting topic, which was first analyzed both theoretically and experimentally by Brandt *et al.* [1]; these differences, denominated vicinage effects in the energy loss, are caused by the interferences between the electronic excitations produced in the target by each molecular constituent. The stopping properties of the target and the characteristics of the projectile (energy, molecular structure and electronic density) determine these vicinage effects.

Several works have been devoted to analyze experimentally the energy loss of different molecular projectiles, ranging from the simplest case H_2^+ [1], to more complex ones, such as O_2^- [2], N_2^+ , and O_2^+ [3], C_n^+ ($n \leq 60$) [4–7], O_2 , B_3 , and C_n ($n=2, 3$) neutral molecules [8], B_n^+ ($n=2-4$) [9], and Si_n^+ ($n \leq 3$) [10]. Most of such studies have shown that the energy lost by the atomic ions resulting from the dissociation of the molecular projectile, randomly oriented with respect to the beam direction, was higher than that of the same but isolated atomic ions [2,4,9]; the opposite result was obtained for diatomic N_2^+ and O_2^+ molecular projectiles with their interatomic axis aligned with respect to the beam direction [3]. A considerable effort has been developed to explain theoretically some of these results [1,3,11–20].

The study of the energy loss of large molecules or clusters [4,21–24] has recently acquired a renewed interest [25–28] because as the number of molecular constituents increases one can check whether the differences in the energy loss with respect to the case of single ions also increases or not. However, to our knowledge there is a lack of a systematic study

covering the range between small- and large-size clusters.

The main aim of this work is to analyze how the cluster size and velocity, as well as the target nature, affect the energy loss of the carbon atomic ions resulting from molecule dissociation, in comparison with isolated carbon atomic ions having the same velocity. This systematic study is interesting in order to state how to get the highest (or the lowest) enhancement in the energy loss of the projectile with respect to the corresponding atomic ions, which may be of practical interest for inertial confinement or radiation therapy.

We make this analysis using a simulation code that includes the electronic interactions (stopping and wake forces) felt by each molecular fragment as well as interactions with nuclei (Coulomb repulsion among molecular fragments and nuclear scattering with target atoms) [29,30]. As most of these interactions depend on the charge state of each fragment, we have included the capture or loss of electrons by molecular fragments when they move through the target. In addition, we take into account the order in which the molecular fragments enter and leave the foil surfaces, so the lack of some of these interactions when the fragments are outside the foil is explicitly taken into account.

Our code follows dynamically the evolution of the molecular constituents after their dissociation, which allows us to know their position and velocity, as well as the charge state at any time; these data are used to evaluate the energy-loss distribution of the fragments that leave the foil and reach a detector with specific characteristics (such as position, angular acceptance, etc.).

In what follows we introduce briefly the simulation code (Sec. II) and discuss our results in Sec. III; finally, we present

our conclusions in Sec. IV. Atomic units will be used throughout this work except where otherwise stated.

II. SIMULATION CODE

Our simulation code [29,30] is based in a combination of molecular dynamics and Monte Carlo techniques. The molecular dynamics treatment consists in numerically solving Newton's equation of motion for all particles that form the system we are analyzing. If we know at the time t the position, the velocity, and the forces that act on each particle moving through a solid, we can calculate their positions and velocities after a time step Δt and, therefore, at any time $t + l\Delta t$, where l is the number of time steps. Molecular dynamics is a deterministic technique but the capture and loss of electrons, the stopping force, and the nuclear scattering, which the projectile suffers, have a stochastic nature. Moreover, we must also consider that each molecular projectile initially impinges on the solid with its structure randomly oriented with respect to the incident velocity. So, to obtain representative results from a statistical point of view we have to simulate the interaction of $\approx 10^5$ atomic ions with the target.

When a swift molecular ion impinges on a solid, it dissociates into its atomic constituents in the first atomic layers of the target [31]. These atomic ions suffer electron-capture and -loss processes until they reach a dynamical equilibrium. During their motion through the solid the atomic ions lose energy due to excitations of the target electrons and nuclear scattering with the target atoms. Moreover, each atomic ion interacts with its fragment partners through the wake forces and the Coulomb repulsion. As a consequence of the latter two interactions, the energy loss of an atomic ion resulting from the dissociation of a molecule can be different than the energy loss of the same, but isolated, atomic ion, giving rise to the so-called vicinage effects in the energy loss. Leaving aside for a moment the nuclear scattering, the total force \mathbf{F}_i , acting on the dissociated i -atomic ion, is given by

$$\mathbf{F}_i = \mathbf{F}_{\text{stopping},i} + \mathbf{F}_{\text{wake},i} + \mathbf{F}_{\text{Coulomb},i}. \quad (1)$$

The stopping force $\mathbf{F}_{\text{stopping},i}$ depends on the charge state of the i -atomic ion; the wake force $\mathbf{F}_{\text{wake},i}$ and the Coulomb repulsion $\mathbf{F}_{\text{Coulomb},i}$ depend on the charge states of both, the i -atomic ion and its neighbor atomic ions. Of course, $\mathbf{F}_{\text{wake},i} = \mathbf{F}_{\text{Coulomb},i} = 0$ when the projectile is an isolated atomic ion.

In the following we describe the inclusion in our simulation code of all the above mentioned interactions.

A. Stopping force

When the i -atomic ion (with atomic number Z_i) is moving with velocity v_i through a solid characterized by an energy-loss function $\text{Im}[-1/\epsilon(k, \omega)]$, it is slowed down by losing energy in electronic excitations of the target (with energy ω and momentum k); $\epsilon(k, \omega)$ is the target dielectric function. This slowing down is characterized by the stopping power

$$S_{p,i} = \frac{2}{\pi v_i^2} \int_0^\infty dk \frac{[Z_i - \rho_i(k)]^2}{k} \int_0^{kv_i} d\omega \omega \text{Im} \left[\frac{-1}{\epsilon(k, \omega)} \right] \quad (2)$$

and the energy-loss straggling

$$\Omega_i^2 = \frac{2}{\pi v_i^2} \int_0^\infty dk \frac{[Z_i - \rho_i(k)]^2}{k} \int_0^{kv_i} d\omega \omega^2 \text{Im} \left[\frac{-1}{\epsilon(k, \omega)} \right], \quad (3)$$

where $\rho_i(k)$ is the Fourier transform of the electronic density of the i -atomic ion. The stopping force that acts on the i -atomic ion fluctuates because of the stochastic nature of the interaction with the target electrons. So the modulus of the stopping force, $F_{\text{stopping},i}$, is given by a Gaussian distribution, for which $S_{p,i}$ is the mean value and $\Omega_i/\sqrt{\Delta s_i}$ is the standard deviation; $\Delta s_i = v_i \Delta t$ is the distance traveled by this atomic ion in a time step Δt . Then

$$\mathbf{F}_{\text{stopping},i} = -[S_{p,i} + (\Omega_i/\sqrt{\Delta s_i})\xi_0]\hat{\mathbf{v}}_i, \quad (4)$$

where ξ_0 is a random number obtained according to a Gaussian distribution [32] and $\hat{\mathbf{v}}_i$ is the unit vector of the instantaneous velocity \mathbf{v}_i .

For medium-size ions, like carbon, $\rho_i(k)$ can be obtained for N_i bound electrons using the Brandt-Kitagawa model [33],

$$\rho_i(k) = \frac{N_i}{1 + (k\Lambda_i)^2}, \quad (5)$$

$\Lambda_i = 0.48N_i^{2/3}/(Z_i - N_i/7)$ being a variational parameter that minimizes the internal energy of the atomic ion; this result practically coincides with that obtained from the Lenz-Jensen model [33]. The Brandt-Kitagawa model [33] is one of the most used descriptions for the electronic charge density of the projectile, because of the straightforwardness of the analytical expressions obtained for $\rho_i(k)$ and the good comparison with experimental data [34].

A realistic description of $\text{Im}[-1/\epsilon(k, \omega)]$ is obtained by combining a sum of Mermin-type [35–39] energy-loss functions that fits to experimental optical data and the use of generalized oscillator strengths [37–39]; these contributions account for excitations of the target outer-shell and inner-shell electrons, respectively.

B. Wake force and Coulomb repulsion

The electronic excitations created in the target by a projectile also affect the motion of its partners, through the so-called wake force [1,40,41]. This force is calculated as stated in Ref. [36] for protons, but now using the Brandt-Kitagawa model [33] to describe the electrons bound to each atomic ion. Using cylindrical coordinates, the wake force acting on the i -atomic ion due to its neighbor, denoted by j , can be decomposed into its parallel and perpendicular components with respect to the velocity \mathbf{v}_j ,

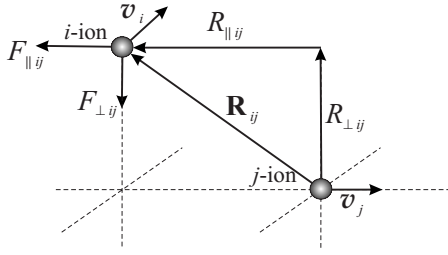


FIG. 1. $F_{\parallel ij}$ and $F_{\perp ij}$ are the parallel and perpendicular components of the wake force, with respect to the velocity \mathbf{v}_j , acting on the i -atomic ion due to its neighbor, denoted by j . $R_{\parallel ij}$ and $R_{\perp ij}$ are the parallel and perpendicular components of the internuclear vector \mathbf{R}_{ij} between the i - and j -atomic ions.

$$F_{\parallel ij} = \frac{2}{\pi v_j^2} \int_0^\infty \frac{dk}{k} [Z_i - \rho_i(k)][Z_j - \rho_j(k)] \times \int_0^{kv_j} d\omega \omega J_0(R_{\perp ij} \sqrt{k^2 - \omega^2/v_j^2}) \times \left\{ \sin\left(\frac{\omega R_{\parallel ij}}{v_j}\right) \text{Re}\left[\frac{1}{\epsilon(k, \omega)} - 1\right] + \cos\left(\frac{\omega R_{\parallel ij}}{v_j}\right) \text{Im}\left[\frac{1}{\epsilon(k, \omega)}\right] \right\} \quad (6)$$

and

$$F_{\perp ij} = \frac{2}{\pi v_j^2} \int_0^\infty \frac{dk}{k} [Z_i - \rho_i(k)][Z_j - \rho_j(k)] \times \int_0^{kv_j} d\omega \sqrt{k^2 - \omega^2/v_j^2} J_1(R_{\perp ij} \sqrt{k^2 - \omega^2/v_j^2}) \times \left\{ \cos\left(\frac{\omega R_{\parallel ij}}{v_j}\right) \text{Re}\left[\frac{1}{\epsilon(k, \omega)} - 1\right] - \sin\left(\frac{\omega R_{\parallel ij}}{v_j}\right) \text{Im}\left[\frac{1}{\epsilon(k, \omega)}\right] \right\}, \quad (7)$$

where $R_{\parallel ij}$ and $R_{\perp ij}$ are the parallel and perpendicular components of the internuclear vector \mathbf{R}_{ij} between the i - and j -atomic ions (see Fig. 1); $J_0(\dots)$ and $J_1(\dots)$ are Bessel functions of the first kind [42].

To simplify the simulations we evaluate Eqs. (6) and (7) using the same velocity for all atomic ions that form the molecular projectile. This is a plausible approximation because the velocities of the atomic ions only become significantly different for large depths inside the target, but in such situations the wake forces are negligible due to the large distance between the molecular constituents, because of the Coulomb repulsion. Leaving aside the evaluation of Eqs. (6) and (7), the different velocities of the atomic ions are properly considered through all the simulation.

The total wake force that acts on the i -atomic ion due to all its neighbors is given by

$$\mathbf{F}_{\text{wake}, i} = \sum_{j \neq i}^n \sqrt{F_{\parallel ij}^2 + F_{\perp ij}^2} \hat{\mathbf{v}}_j, \quad (8)$$

where n is the number of atomic ions that constitutes the molecular projectile. It is important to note that for a given target, the stopping force depends on the projectile velocity and charge state, Eqs. (2)–(4), but the wake force depends also on the positions and velocities of the rest of the atomic ions resulting from the cluster dissociation, Eqs. (6)–(8).

The mutual repulsion between charged neighbors is considered by means of a pure Coulomb potential, which gives the following force acting on the i -atomic ion:

$$\mathbf{F}_{\text{Coulomb}, i} = (Z_i - N_i) \sum_{j \neq i}^n \frac{(Z_j - N_j)}{R_{ij}^2} \hat{\mathbf{R}}_{ij} = q_i \sum_{j \neq i}^n \frac{q_j}{R_{ij}^2} \hat{\mathbf{R}}_{ij}, \quad (9)$$

where $q_i = Z_i - N_i$ is the charge state of the i -atomic ion (analogously for the j -atomic ion) and $\hat{\mathbf{R}}_{ij}$ is the unit vector of \mathbf{R}_{ij} .

C. Nuclear scattering

Multiple scattering of an atomic ion with the target atomic cores is considered through a Monte Carlo model [43,44], using the universal potential cross section [34] to calculate the scattering angles and the corresponding nuclear energy loss. In this treatment the reduced path length between two successive collisions is given by

$$\mathcal{L} = \frac{-4\mu \ln(\xi_1)}{m_1 + m_2 \mathcal{J}_{\text{tot}}}, \quad (10)$$

where ξ_1 is a random number uniformly distributed between 0 and 1; m_1 and m_2 are the projectile and target atomic masses, respectively; μ is the reduced mass, and $\mathcal{J}_{\text{tot}} = 1/(4N^{2/3}a_U^2)$ is an estimation of the reduced total cross section, \mathcal{N} being the target atomic density and a_U the universal screening length [34],

$$a_U = \frac{0.8853}{Z_i^{0.23} + \mathcal{Z}^{0.23}}, \quad (11)$$

where Z_i and \mathcal{Z} are the projectile and target atomic numbers. The path length L between two successive collisions is directly related to \mathcal{L} by means of

$$L = \frac{m_1 + m_2}{4\pi a_U^2 \mu \mathcal{N}} \mathcal{L}. \quad (12)$$

The polar scattering angle θ relative to the ion direction of motion is given as a function of the parameter η through

$$\cos \theta = \left(1 - \frac{2\mu\eta^2}{m_1\mathcal{E}^2}\right) \left[1 - \frac{4\mu\eta^2}{(m_1 + m_2)\mathcal{E}^2}\right]^{-1/2}, \quad (13)$$

where \mathcal{E} is the reduced energy defined by

$$\mathcal{E} = \frac{a_U m_2}{Z_1 Z_2 (m_1 + m_2)} E, \quad (14)$$

E being the projectile instantaneous energy.

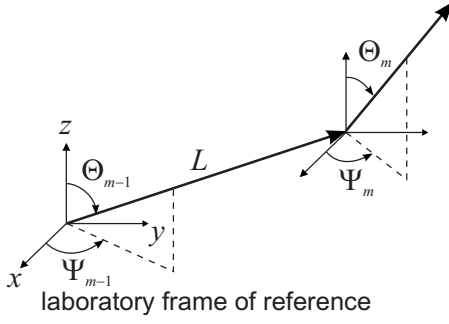


FIG. 2. Angles in the laboratory frame of reference that determine the projectile direction of motion before $(\Theta_{m-1}, \Psi_{m-1})$ and after (Θ_m, Ψ_m) the m collision. L is the distance between successive collisions.

The value of the parameter η is calculated using

$$\mathcal{J}(\eta) = \mathcal{J}(\mathcal{E}) + \xi_2 \mathcal{J}_{\text{tot}}, \quad (15)$$

where ξ_2 is a random number, uniformly distributed between 0 and 1. The scattering cross section in reduced units, $\mathcal{J}(\eta)$, can be evaluated using

$$\mathcal{J}(\eta) = \mathcal{J}(\eta_0) + \int_{\eta_0}^{\eta} d\eta' \frac{f(\eta')}{\eta'^2}, \quad (16)$$

where $f(\eta)$ is the function given by Meyer [45] and we assume $\eta_0 = 10^{-4}$ as a fixed lower integration limit. Equation (15) is independent of η_0 , because both $\mathcal{J}(\eta)$ and $\mathcal{J}(\mathcal{E})$ depend on η_0 through Eq. (16).

Finally, the azimuthal scattering angle ψ relative to the ion direction of motion is evaluated as

$$\psi = 2\pi\xi_3, \quad (17)$$

where ξ_3 is a random number uniformly distributed between 0 and 1.

Figure 2 sketches the motion of an atomic ion before the m collision, in a direction defined by the polar angle Θ_{m-1} and the azimuthal angle Ψ_{m-1} in the laboratory frame of reference. We obtain L by means of Eq. (12); after an elapsed time L/v , the m collision takes place and we determine the scattering angles θ and ψ using the Monte Carlo technique. The new direction of the projectile after the m collision is defined by [44,46]

$$\cos \Theta_m = -\sin \theta \cos \psi \sin \Theta_{m-1} + \cos \theta \cos \Theta_{m-1},$$

$$\begin{aligned} \cos \Psi_m = & \frac{1}{\sin \Theta_m} (\sin \theta \cos \psi \cos \Theta_{m-1} \cos \Psi_{m-1} \\ & - \sin \theta \sin \psi \sin \Theta_{m-1} \cos \Psi_{m-1}). \end{aligned} \quad (18)$$

D. Electron capture and loss

The capture and loss of electrons by the dissociated atomic ions have been incorporated in our simulation code using a model similar to that suggested in Ref. [44]. We

assume that the electron-loss cross section $\sigma_{\text{loss},i}$ for the i -atomic ion is proportional to the number of bound electrons $N_i = Z_i - q_i$,

$$\sigma_{\text{loss},i}(q_i \rightarrow q_i + 1) = (Z_i - q_i)\sigma_i, \quad (19)$$

where $q_i \rightarrow q_i + 1$ denotes that the atomic ion changes its charge state from q_i to $q_i + 1$ and σ_i is the geometrical cross section of the i -atomic ion,

$$\sigma_i = \pi \langle r_i \rangle^2 = 4\pi\Lambda_i^2, \quad (20)$$

with $\langle r_i \rangle = 2\Lambda_i$ being the average distance between the bound electrons and the atomic nucleus in the Brandt-Kitagawa model [33].

The inverse mean free path for electron loss is

$$\mu_{\text{loss},i}(q_i \rightarrow q_i + 1) = \mathcal{N}\sigma_{\text{loss},i}(q_i \rightarrow q_i + 1). \quad (21)$$

If multiple-electron processes are neglected, the inverse mean free path for electron capture from the equilibrium relation is

$$\mu_{\text{capt},i}(q_i + 1 \rightarrow q_i) = \frac{\phi(q_i)}{\phi(q_i + 1)} \mu_{\text{loss},i}(q_i \rightarrow q_i + 1), \quad (22)$$

where $\phi(q_i)$ and $\phi(q_i + 1)$ are the equilibrium fractions of the q_i and $q_i + 1$ charge states, respectively. Then the probability of electron loss, $P_{\text{loss},i}$ (or electron capture, $P_{\text{capt},i}$), by the i -atomic ion with charge state q_i is

$$P_{\text{loss},i}(q_i \rightarrow q_i + 1) = \frac{\mu_{\text{loss},i}(q_i \rightarrow q_i + 1)}{\mu_{\text{capt},i}(q_i \rightarrow q_i - 1) + \mu_{\text{loss},i}(q_i \rightarrow q_i + 1)}, \quad (23)$$

$$P_{\text{capt},i}(q_i \rightarrow q_i - 1) = 1 - P_{\text{loss},i}(q_i \rightarrow q_i + 1). \quad (24)$$

According to these probabilities our simulation code chooses at each time step whether the i -atomic ion loses or captures an electron.

To satisfy the normalization condition $\sum_{q_i=0}^{Z_i} \phi(q_i) = 1$, each charge state fraction $\phi(q_i)$ of the i -atomic ion is evaluated through

$$\phi(q_i) = \frac{f(q_i)}{Z_i \sum_{q_i=0}^{Z_i} f(q_i)}, \quad (25)$$

where the distribution of charge states with $\langle q_i \rangle$ mean equilibrium charge state and σ_i standard deviation is given by

$$f(q_i) = \frac{1}{\sqrt{2\pi\sigma_i^2}} \exp\left[-\frac{(q_i - \langle q_i \rangle)^2}{2\sigma_i^2}\right]. \quad (26)$$

Both $\langle q_i \rangle$ and σ_i are obtained through a fit to experimental data [47] and depend on Z_i , v_i , and on the target atomic number \mathcal{Z} .

III. RESULTS

Taking into account all the ingredients presented above, we can obtain the coordinates and velocities of any atomic

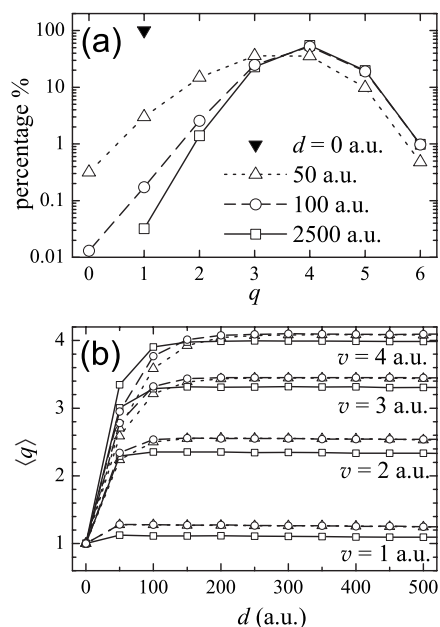


FIG. 3. (a) Preequilibrium charge-state distributions of carbon ions incident as C^+ with $v=4$ a.u. on an amorphous carbon foil. The target depth d is indicated in the legend. (b) Average charge state $\langle q \rangle$, as a function of the depth d , of carbon atomic ions incident as C^+ with different velocities on an (\square) amorphous carbon, (\circ) aluminum, and (\triangle) silicon targets. The lines in both figures are drawn only to guide the eye.

ion at any time. In order to simplify the writing and when no confusion results, we remove in the following the subscripts i and j , used through Sec. II to state the model.

A. Isolated atomic ions

As previously stated, atomic ions moving through a solid suffer electron-capture and -loss processes until they reach a dynamical equilibrium. Our simulation code provides the charge-state distributions as a function of the depth d inside the foil. Notice that $d \neq vt$, because the direction of the atomic ion velocity \mathbf{v} changes with the elapsed time t . Figure 3(a) shows the charge-state distributions before equilibrium is reached for C^+ incident with $v=4$ a.u. on a carbon foil—i.e., the preequilibrium charge-state distributions. According to Fig. 3(a), equilibrium is acquired after a depth of ~ 100 a.u.; the most probable charge states are C^{4+} , C^{3+} , and C^{5+} , with the probability of finding the atomic ions in another charge-state being negligible. Our equilibrium charge state distributions coincide with the ones given by the CASP code [47], because such equilibrium is imposed through Eq. (22). Improving the evaluation of σ_{loss} only will affect the transient time needed to acquire the equilibrium charge-state distribution, which is independent of σ_{loss} once equilibrium is reached.

The evolution of this dynamical equilibrium can also be observed in Fig. 3(b), where we depict the average charge state $\langle q \rangle$ of the carbon projectiles (incident as C^+) as a function of the target depth d for different projectile velocities and targets. According to the figure, the average charge re-

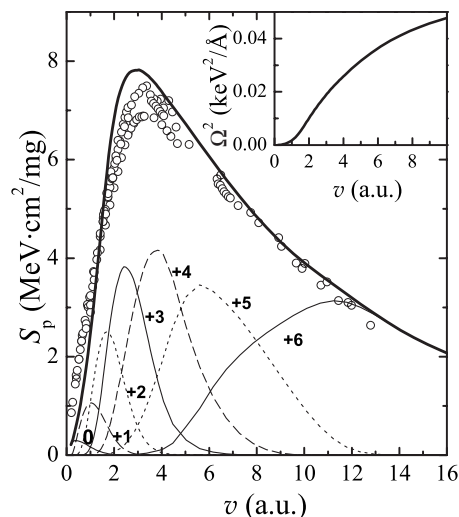


FIG. 4. Stopping power of amorphous carbon for carbon atomic ions, as a function of the projectile velocity. The thick solid curve represents our calculations, Eqs. (2) and (27), and symbols are a collection of experimental data [49]; the thin line curves labeled 0, +1, +2, ..., +6 are the contributions to the stopping power due to each charge state of the carbon ion. The inset shows the calculated energy-loss straggling per unit path length, using Eqs. (3) and (28).

mains practically constant for all cases after a depth of ~ 150 a.u. The transient time slightly depends on the target nature, but strongly on the projectile velocity.

The energy loss of an atomic ion moving through a solid is characterized by the stopping power and the energy loss straggling [48]

$$S_p = \sum_{q_i=0}^{Z_i} \phi(q_i) S_{p,i}, \quad (27)$$

$$\Omega^2 = \sum_{q_i=0}^{Z_i} \phi(q_i) \Omega_i^2, \quad (28)$$

where $S_{p,i}$ and Ω_i^2 come from Eqs. (2) and (3), respectively, and the charge fractions are derived from Eq. (25). Figure 4 depicts S_p and Ω^2 of amorphous carbon for swift carbon ions. The symbols are experimental data [49], and the thick solid lines correspond to our calculations. The contributions to the stopping power due to the different charge states q_i of the projectile—i.e., $\phi(q_i) S_{p,i}$ —are represented by different types of thin lines, the labels indicating the corresponding charge state. Similar results were obtained for silicon and aluminum targets. In all cases considered in this work there is a satisfactory agreement between our calculations and the experimental data in a broad range of projectile velocities.

B. Dissociated atomic ions

The charge state of a swift atomic ion moving through a solid is different when it is isolated or when it forms part of a molecular projectile. In general, for a given velocity the average charge state of a dissociated atomic ion is lower than

that of an isolated atomic ion and it depends on the molecular structure and velocity, as well as on the foil composition and thickness [17,50–57]. These vicinage effects in the charge state are related to the proximity of the neighboring atomic ions as they move through the target.

Recent experiments [53,55] show that dissociated atomic ions have smaller charge state than the corresponding isolated ions. We obtained in Ref. [57] that the reduction in charge state inside the target is lower than that experimentally measured just at the exit of the foil. That reduction scarcely affects the energy loss of the dissociated atomic ions [58]. Therefore we assume in this work that the charge state of each atomic ion resulting from the molecular dissociation is identical to that corresponding to the same atomic (but isolated) ion.

The energy loss of the atomic ions resulting from the dissociation of a cluster depends on its size, geometry, and velocity, as well as on the target nature. The differences between the energy loss of a cluster and the sum of the energy loss of each one of its constituents moving with the same velocity but isolated—namely, the vicinage effects in the energy loss—are quantified through the stopping power ratio

$$\mathcal{R} = \frac{\Delta E(C_n^+)}{n\Delta E(C^+)}, \quad (29)$$

where $\Delta E(C_n^+)$ and $\Delta E(C^+)$ are the energy lost by the C_n^+ cluster and an isostachic C^+ ion, respectively; n is the number of atoms that form the cluster.

To analyze the dependence of the vicinage effects in the energy loss with the projectile size and geometrical structure, we have calculated the energy loss of C_n^+ clusters ($n=2-60$) moving through amorphous carbon, aluminum, and silicon foils. These values of n cover wide types of geometries: linear ($n=2-8$) [59–63], ring-shaped ($n=3, 10$) [64], and cage-like structures ($n \geq 20$) [64,65]. The geometrical structures of a few representative clusters are depicted in Fig. 5.

We show in Fig. 6 the stopping power ratio \mathcal{R} as a function of the target thickness d for C_n^+ ($n=3, 10, 20, 36, 60$) clusters incident with velocities $v=1, 2, 3,$ and 4 a.u. on amorphous carbon, aluminum, and silicon foils. A linear structure for the C_3^+ has been assumed in order to analyze the transition between the different geometries. Curves corresponding to C_n^+ ions with $n=2, 4-8, 28,$ and 50 have been omitted for clarity reasons, since they do not report any additional feature.

For almost all cluster sizes, velocities, and foil thicknesses, $\mathcal{R} > 1$. This trend is not satisfied for the thinner foils, where $\mathcal{R} < 1$. Such behavior, more noticeable for low v , could be attributed to the different initial charge states of the C^+ as compared to those of the dissociated atomic ions ($n-1$ neutral C atoms and one C^+ ion, for a C_n^+ cluster). In addition, $\mathcal{R} \rightarrow 1$ the thicker is the foil and the lower is the velocity, so the vicinage effects in the energy loss decrease when the dwell time increases. This is due to two factors that increase the interatomic distances and, therefore, distort the correlated motion of the cluster fragments: (i) the nuclear

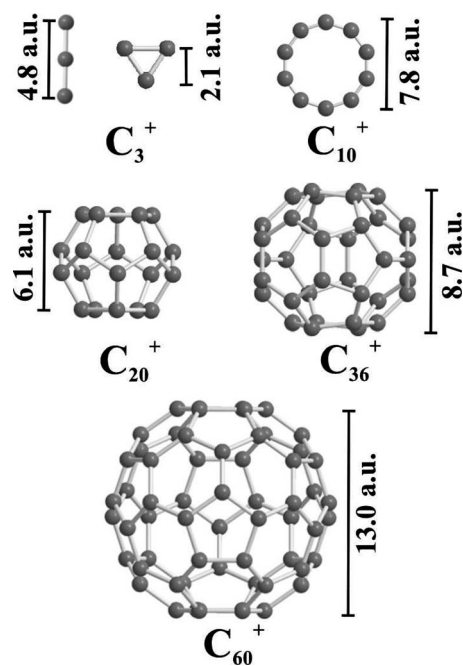


FIG. 5. Geometrical structures of some representative C_n^+ clusters that we have used in our calculations: $n=3$ and 10 [64], $n=20, 36,$ and 60 [65].

scattering (more important for the thicker foils) and (ii) the Coulomb explosion (more significant for the thinner foils).

The vicinage effects in the energy loss also depend on the cluster velocity v ; the value of \mathcal{R} clearly increases with v . For instance, $\mathcal{R} \sim 3$ for C_{60}^+ moving with $v=4$ a.u. through ~ 500 -a.u. aluminum foil. Moreover, the energy-loss enhancement of the C_n^+ clusters strongly depends on the target nature, being more important for silicon or aluminum foils than for amorphous carbon. This behavior is due to the larger extension of the wake forces induced in silicon and aluminum compared with the ones in amorphous carbon, as can be seen in Fig. 7 and in Refs. [36,66].

On the other hand, for amorphous carbon foils there is a sizable increase in the stopping power ratio with the cluster size for $n=3-20$, which is due not only to the increase of n , but also to the change of structure (linear, ring-shaped, or cage-like); the combined effect of both factors increases the number of neighbors around each atomic ion, with the consequent enhancement of interactions, and the corresponding vicinage effects, felt by the atomic ions. Figure 6 shows no important differences in value of \mathcal{R} for the case of C_n^+ clusters in amorphous carbon foils when n increases even more ($n=20-60$). We have also observed this tendency for C_{28}^+ and C_{50}^+ ions. The absence of a significant variation for the stopping power ratio \mathcal{R} in this case can be explained in terms of cancellations of vicinage effects due to the presence of several atomic ions at different distances from a given atomic ion.

A deviation of this general trend is observed for silicon and aluminum foils; for instance, $\mathcal{R}(C_3^+) > \mathcal{R}(C_n^+)$ with $v=1$ a.u., whatever the value of n was. This anomaly is also observed for C_{20}^+ with $v=2$ a.u. In addition, it is worth noticing for such targets the different shape of the \mathcal{R} curves for

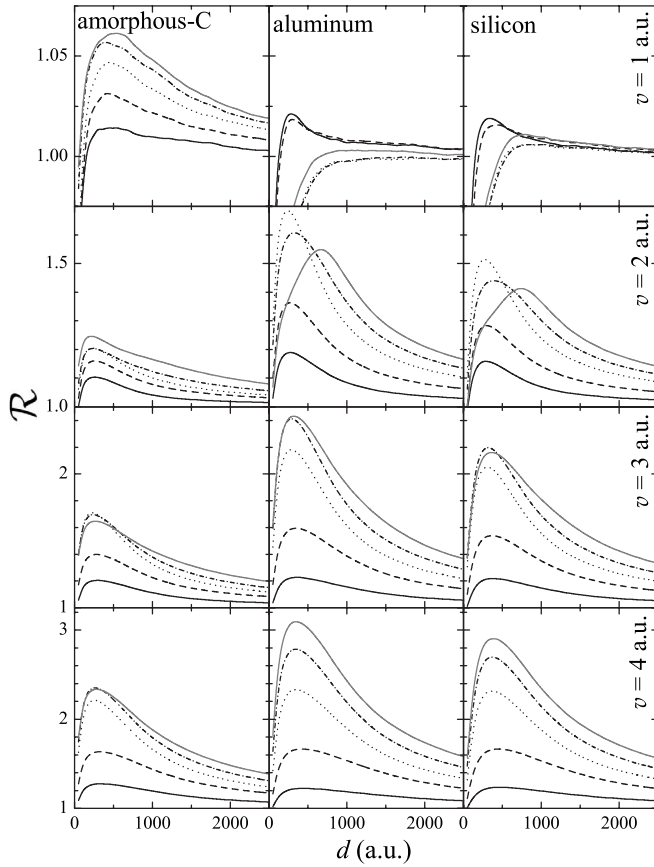


FIG. 6. Stopping power ratio \mathcal{R} for several target materials, cluster velocities, and sizes, as a function of the foil thickness d . The cluster velocity and target material are indicated as different rows and columns, respectively. The different types of curves indicate the cluster size: $n=3$ (solid lines), $n=10$ (dashed lines), $n=20$ (dotted lines), $n=36$ (dot-dashed lines), and $n=60$ (gray lines).

C_{60}^+ ions in relation to those for C_n^+ ($n=3, 10, 20$, and 36) ions, both with velocity $v=2$ a.u.; the slope of the stopping power ratio clearly changes for C_{60}^+ when $200 \lesssim d \lesssim 800$ a.u. This change of slope also is observed for C_{50}^+ ions.

To explain this behavior we show in Fig. 7 the wake forces F_{\parallel} and F_{\perp} that act on a C^{2+} ion (partner ion) due to another C^{2+} ion (leading ion, located at the origin of the graph) as a function of the distance R_{\parallel} , both moving with $v=2$ a.u. through amorphous carbon or silicon targets. We have chosen the most probable charge state ($q=2$) for $v=2$ a.u. [see Fig. 3(b)]. We depict the distribution of interatomic distances for C_{60}^+ at $d=500$ a.u. (where the change in the slope of \mathcal{R} is more pronounced) to help us in determining the most probable interatomic distances between atomic ions. The wake forces F_{\parallel} and F_{\perp} are shown for $0.25 \leq R_{\perp} \leq 5$ a.u. because the more important contribution to the total wake force felt by the partner ion comes from such small values of R_{\perp} (contributions coming from larger values of R_{\perp} can be neglected in a qualitative discussion).

According to the figure, $F_{\parallel}, F_{\perp} < 0$ and show a similar behavior in front of the leading ion for both amorphous carbon and silicon targets. On the contrary, differences on the wake forces appear behind the leading ion: generally $F_{\parallel} > 0$

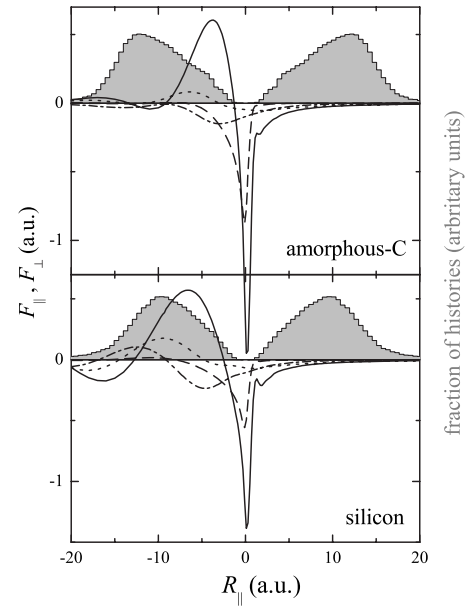


FIG. 7. Left axis: parallel and perpendicular components of the wake forces that act on a C^{2+} ion due to a neighbor C^{2+} ion (located at the origin of the graph, $R_{\parallel}=0$), as a function of the parallel component R_{\parallel} of the interatomic distance; both ions moving with $v=2$ a.u. through amorphous carbon or silicon foils. The meaning of the lines are (solid line) F_{\parallel} for $R_{\perp}=0.25$ a.u., (dashed line) F_{\perp} for $R_{\perp}=0.25$ a.u., (dotted line) F_{\parallel} for $R_{\perp}=5$ a.u., and (dot-dashed line) F_{\perp} for $R_{\perp}=5$ a.u. Right axis: the interatomic distance distributions of C_{60}^+ at $d=500$ a.u. are depicted as shaded histograms.

for amorphous carbon, whereas F_{\parallel} for silicon can have both positive and negative values. In addition, $F_{\perp} < 0$ for amorphous carbon, whatever the partner ion is, but for silicon targets it can be positive or negative. Such negative values of F_{\perp} for amorphous carbon tend to align the partner ions, whereas the positive values of F_{\perp} for silicon give rise to a nonalignment effect. So the wake forces F_{\parallel} and F_{\perp} that act on the partner ion can be positive or negative behind the leading ion for silicon targets, compensating themselves and giving rise to cancellation effects in the energy loss; such a cancellation is not observed for amorphous carbon foils, because almost always $F_{\parallel} > 0$ or $F_{\perp} < 0$ behind the leading ion, as can be noticed in Fig. 7. These cancellation effects are responsible for the observed reduction of \mathcal{R} for C_{60}^+ in silicon when $200 \lesssim d \lesssim 800$ a.u.

The dependence of \mathcal{R} on the cluster size n is illustrated in Fig. 8 for C_n^+ ($n=2-60$) clusters moving through several foil thicknesses. The same graphs are depicted in the insets, but without breaking the horizontal axis; the scale of the vertical axis is identical to those of the corresponding main graph. The purpose of these insets is to show more clearly the dependence on n . For amorphous carbon foils \mathcal{R} increases with n for the smaller clusters ($n=2-20$), but it remains almost constant for the larger clusters ($n=20-60$). However, for silicon and aluminum foils there is a maximum of \mathcal{R} for C_3^+ with $v=1$ a.u. and for C_{20}^+ with $v=2$ a.u., which only is observed for the thinner foils ($d=250$ a.u.); the maximum of the stopping power ratio is moved to larger clusters as the velocity increases. This anomaly, which can

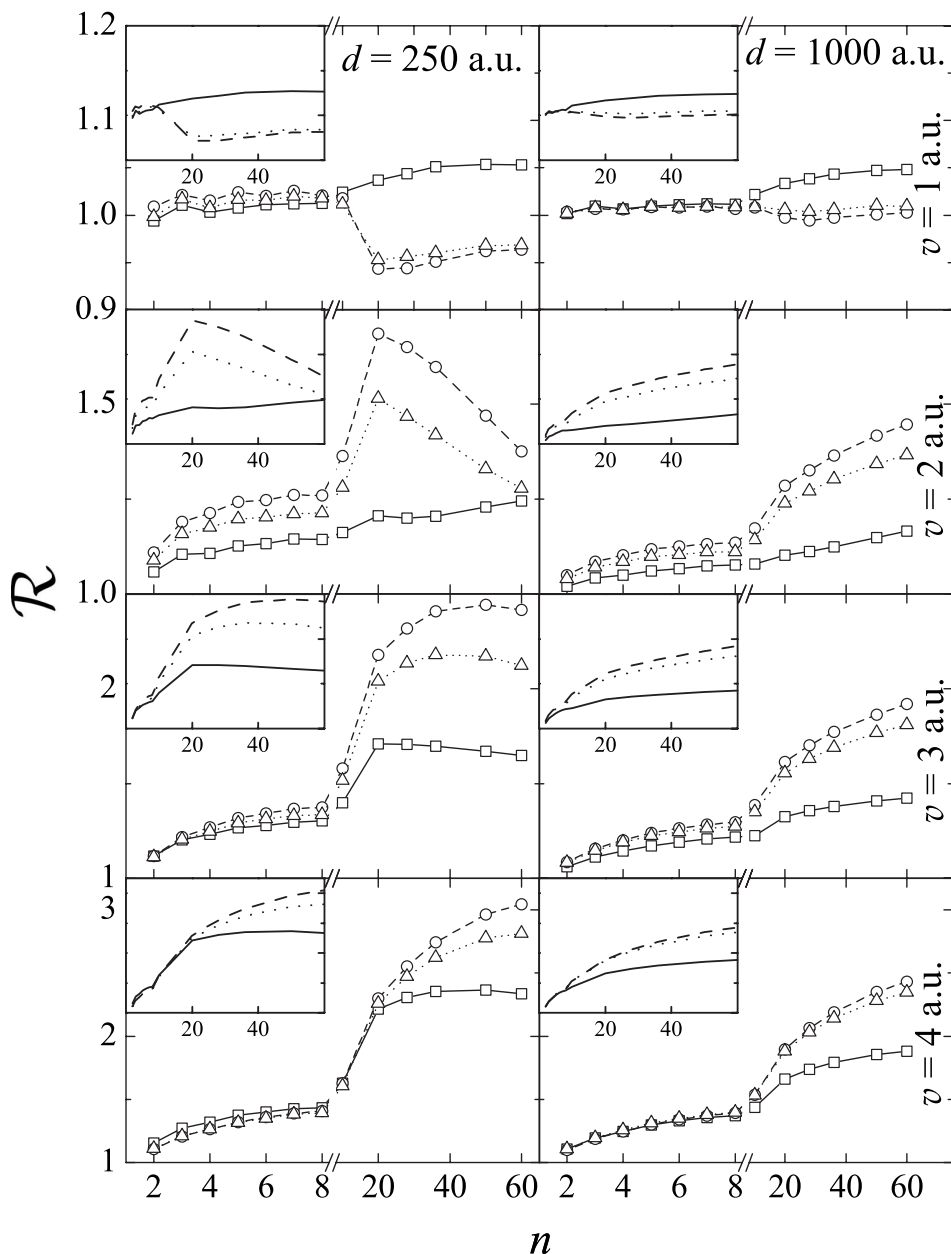


FIG. 8. Stopping power ratio \mathcal{R} as a function of the number n of atomic ions that constitutes the cluster, for different projectile velocities and target materials: (\square) amorphous carbon, (\circ) aluminum, and (\triangle) silicon. The target thickness d and projectile velocity v are indicated in the figure. The lines joining the symbols are drawn only to guide the eye. The insets show the behavior of \mathcal{R} without the break in the horizontal axis; note that the vertical scale in each inset coincides with that in the main graph.

be explained according to the reasoning presented above, is not observed for thicker foils, where the stopping power ratio increases with the number n of constituents.

In conclusion, the number of atomic ions and the geometrical structure of the cluster affect the vicinage effects in the energy loss. In general one could expect that \mathcal{R} increases with the size n of the cluster. However, this tendency cannot be observed for the larger clusters due to the cancellation of the vicinage effects, which arises from the different interatomic distances of the atomic ions that produce positive and/or negative vicinage effects in the energy loss [67].

C. Comparison with experimental data

Baudin *et al.* [4,6] measured the energy loss of C_n^+ ($n=2-8$) ions incident with energy $E_0=1.01-5.65$ MeV/atom on 250-Å-thick amorphous carbon foils, finding slight vicin-

nage effects in the energy loss of the molecular projectiles compared to the same but isolated atomic ions. However, they did not detect (compatible with their experimental resolution of 5%) vicinage effects for C_{60}^+ clusters incident with $E_0=305$ and 455 keV/atom on 300- and 500-Å-thick amorphous carbon foils. Tomaschko *et al.* [5] also reported measurements on the energy loss of small carbon clusters C_n^+ ($n=2-5$) incident with $E_0=1.4-4.0$ MeV on amorphous carbon, Formvar, and gold foils. Contrary to what was observed by Baudin *et al.* [4,6], they did not detect vicinage effects in the energy loss, according to the error bars of their measurements. Besides the stopping power ratio, in order to quantify vicinage effects in the energy loss we use the difference between the mean energy loss of each molecular fragment resulting from the dissociation of C_n^+ and that of the isolated atomic ions,

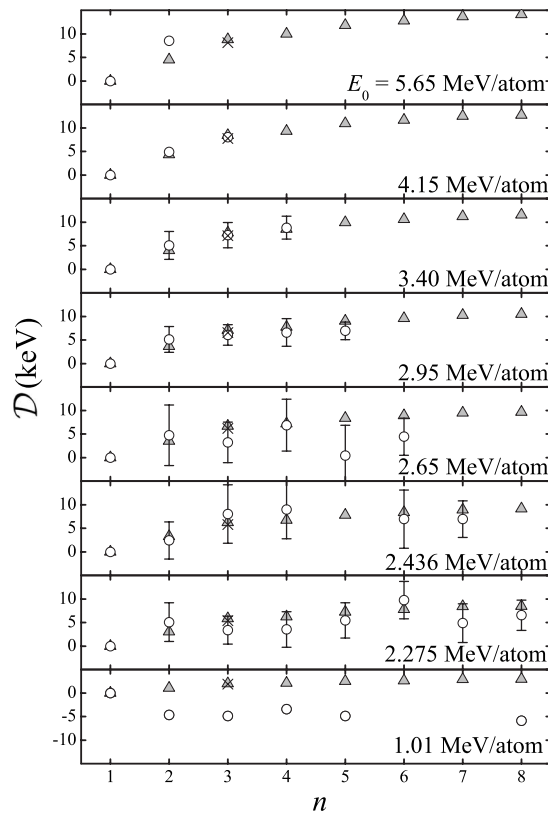


FIG. 9. Difference \mathcal{D} between the mean energy loss of each molecular fragment resulting from the dissociation of a C_n^+ ($n=2-8$) ion and that of the isolated carbon atomic ions, as a function of the number n of atomic ions that constitutes the cluster, incident with different projectile energies E_0 (indicated in the legend of the figure) on 250-Å-thick amorphous carbon foils. The open circles (and the error bars) represent the experimental data [4,6], whereas gray triangles correspond to our results. The crosses represent the results for the C_3^+ cluster when we assume a linear structure.

$$\mathcal{D} = \frac{\Delta E(C_n^+)}{n} - \Delta E(C^+). \quad (30)$$

In Fig. 9 we show \mathcal{D} for small C_n^+ ($n=2-8$) ions incident with energy $E_0=1.01-5.65$ MeV/atom on 250-Å-thick amorphous carbon foils. We have done our simulations using the geometrical structures of the C_n^+ ($n=2-8$) ions in the ground state: bent for C_3^+ [64] and linear for the rest of the molecular ions [59–63]. The open circles and the corresponding error bars represent the experimental data [4,6], whereas gray triangles correspond to our results. The crosses represent the corresponding results when we assume a linear structure for the C_3^+ cluster.

An enhancement in the energy loss of the cluster compared to that of its isolated constituents is observed for $E_0 \geq 2$ MeV/atom. The agreement of our calculations and the experimental data is fairly good for all the experimental situations analyzed, except for the lowest projectile energy ($E_0=1.01$ MeV/atom), where the behavior shown by these measurements [6] differs significantly from the rest of experimental data [4].

When considering in our calculations a linear structure for the C_3^+ ion small differences in \mathcal{D} (lower than 8%) appear,

both being calculations (with a triangular or a linear structure) within the error bars; so from these results it is not possible to state the geometry of the cluster in the experiment. The Coulomb explosion imaging technique [41,68] or the charge-state distributions of the dissociated atomic ions at the exit of the target [53,55–57,69] could be used for this purpose.

As expected, \mathcal{D} increases with the number n of atomic constituents and also grows as the projectile energy becomes higher. Such a dependence with the projectile energy explains why no enhancement in the energy loss was observed by Tomaschko *et al.* [5], since the projectile energies in their experiments were lower than those of the projectiles used by Baudin *et al.* [4].

Recently, Kaneko [17] has reported an analytical calculation of the energy loss of swift C_n^+ ($n=2-8$) ions incident on amorphous carbon foils, obtaining a good agreement with the experimental data [4,6]. According to that model, the electron binding energy of an atomic ion that is part of an ensemble of correlated atomic ions is higher than for an isolated atomic projectile [17]. This effect was evaluated using a pure Coulomb potential for the interaction between the dissociated atomic ions [17], which does not seem a plausible approximation because screening by the target electrons is not considered [56,57]. In addition, these calculations did not take into account the multiple scattering with the target nuclei or how the wake forces affect the motion of the dissociated atomic ions [17]; those effects have been proven to be determinant to explain the correlated motion of the dissociated fragments [41]. The variation in the charge state of the dissociated atomic ions before the equilibrium is acquired (i.e., the transient charge state) also was neglected [17], although the need for considering that effect was previously reported when evaluating the energy loss of swift molecular projectiles traversing thin foils [12,16]. On the contrary, our simulation code includes multiple scattering with the target nuclei, the wake forces, and the transient charge state; it does not include vicinage effects in the charge state, but as we have previously stated, these effects only represent a decrease of less than 5% in the stopping power ratio for the most unfavorable case discussed in this work.

Concerning the experiment performed for C_{60}^+ incident with $E_0=305$ and 455 keV/atom on 300- and 500-Å-thick amorphous carbon foils [4], we depict in Fig. 10 the energy distribution of the dissociated atomic ions compared with that of isolated carbon atomic ions: they are plotted just at the exit of the foil, not when the particles reach a far detector, in order to compare the characteristics of both types of distributions (for dissociated and isolated ions). Nevertheless, the mean energies of these distributions will not change if measured in the detector, because Coulomb explosion (the only interaction) during the travel to the detector broadens the energy distribution without changing its mean energy. Two main features can be seen in these distributions: the ones corresponding to dissociated atomic ions are almost two times wider, and with a smaller mean energy, than the ones for isolated carbon atomic ions. The broadening of the energy distribution can be understood in terms of Coulomb repulsion inside the foil, which accelerates the leading fragments and slows down the trailing ones.

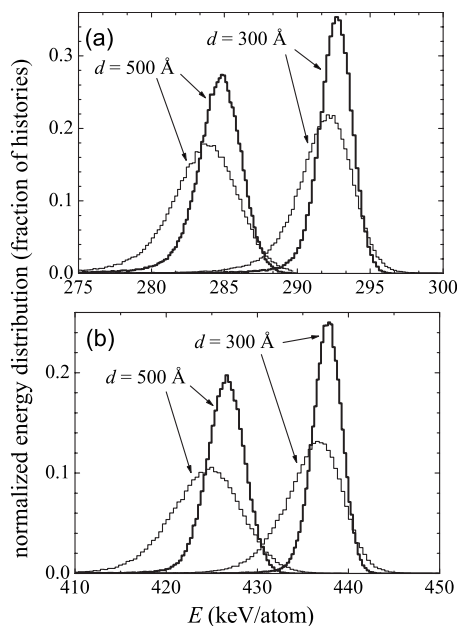


FIG. 10. Energy distribution of carbon atomic ions, (thick lines) isolated and (thin lines) dissociated from C_{60}^+ , when traversing amorphous carbon foils of thickness $d=300$ and 500 Å with incident energies (a) $E_0=305$ and (b) 455 keV/atom. The parameters characterizing the beam and the target correspond to those in the work of Baudin *et al.* [4].

Figure 11 shows \mathcal{R} and \mathcal{D} as a function of the foil thickness for two incident energies: $E_0=305$ and 455 keV/atom. As expected, \mathcal{R} decreases with the foil thickness and tends to one, the thicker the foil. On the other hand, \mathcal{D} grows for the thicker foils, but it is very small, being $\approx 1\%$ of the initial energy per atomic ion, for the two foil thicknesses (300 and

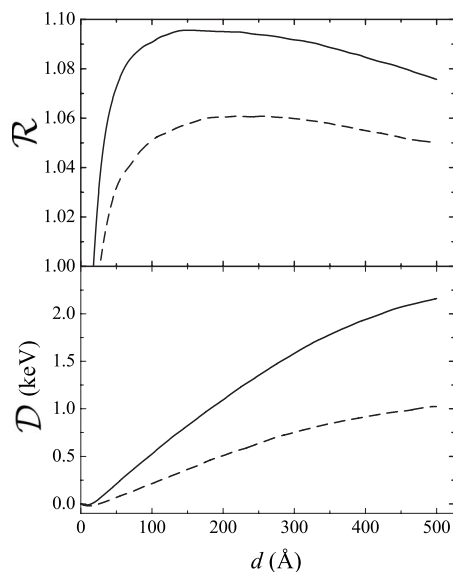


FIG. 11. Dependence with the amorphous carbon foil thickness d of the calculated stopping power ratio \mathcal{R} and the energy-loss difference \mathcal{D} between fragments of C_{60}^+ and carbon atomic ions, both having the same incident energy: (solid lines) $E_0=305$ keV/atom and (dashed lines) $E_0=455$ keV/atom.

500 Å) corresponding to the experimental data [4], and it slowly grows as the foil gets thicker. Therefore, our simulations predict a small enhancement in the energy loss of the dissociated atomic ions in comparison with the isolated ones, which is in good agreement with the experimental observations [4]. All the same, the behavior of both curves \mathcal{R} and \mathcal{D} show that vicinage effects in the energy loss decrease when the foil thickness increases.

IV. CONCLUSIONS

We have calculated the energy loss of swift C_n^+ ($n=2-60$) clusters moving with velocities $1 \leq v \leq 4$ a.u. in amorphous carbon, aluminum, and silicon foils.

Our simulations predict $\mathcal{R} > 1$ in most of the cases analyzed. These vicinage effects in the energy loss usually increase with the projectile size and velocity and also depend on the target nature, being more important for silicon and aluminum foils than for amorphous carbon foils. Then, molecular projectiles incident with high energy in silicon or aluminum thin foils should be used in order to measure the highest enhancement in their energy loss with respect to the corresponding atomic ions. Projectiles with high energy loss could be of interest in inertial confinement fusion [26,27]. However, contrary to what can be expected, the largest molecular projectile does not produce the highest enhancement in the energy loss. With our computer code a systematic study could be made in each particular situation to find out which molecular projectile is the best choice to deposit a high density of energy in the target.

For large molecular projectiles we have observed a cancellation of the wake forces acting on each fragment due to the wide distribution of interatomic distances between the dissociated atomic ions, as was suggested in Ref. [67]; then, \mathcal{R} can decrease or saturate to a constant value when the number of constituents of the cluster increases. For instance, there is a maximum value $\mathcal{R} \sim 1.7$ for C_{20}^+ ions moving with $v=2$ a.u. through aluminum foils.

In addition, we have obtained a satisfactory agreement between our calculations and the experimental data for the energy loss of C_n^+ ($n=2-8$) ions incident with energy $E_0 = 1.01-5.65$ MeV/atom on 250 -Å-thick amorphous carbon foils (except for the lowest energy), where significant vicinage effects in the energy loss were experimentally detected [4,6]. Nevertheless, our simulations only predict a small enhancement ($\sim 1\%$) in the energy loss of C_{60}^+ clusters incident with $v \sim 1$ a.u. in amorphous carbon foils of 300 and 500 Å thicknesses, in accordance with the experimental observation, where no energy-loss enhancement was detected within 5% of experimental limit of observation [4]. This lack of sizable energy-loss differences between fragments of large molecules or clusters and individual atomic ions may be understood in terms of the loss of spatial correlation of the former due to Coulomb repulsion and nuclear scattering, which increase the interatomic distances between the dissociated fragments.

ACKNOWLEDGMENTS

This work was supported by the Spanish Ministerio de

Educación y Ciencia (Projects Nos. FIS2006–13309–C02–01, FIS2006–13309–C02–02, BFM2003–04457–C02–01,

and BFM2003–04457–C02–02). S.H.A. thanks the Fundación Cajamurcia for a research postdoctoral grant.

-
- [1] W. Brandt, A. Ratkowski, and R. H. Ritchie, *Phys. Rev. Lett.* **33**, 1325 (1974).
- [2] J. W. Tape, W. M. Gibson, J. Remillieux, R. Laubert, and H. E. Wegner, *Nucl. Instrum. Methods* **132**, 75 (1976).
- [3] M. F. Steuer, D. S. Gemmell, E. P. Kanter, E. A. Johnson, and B. J. Zabransky, *Nucl. Instrum. Methods Phys. Res.* **194**, 277 (1982).
- [4] K. Baudin, A. Brunelle, M. Chabot, S. Della-Negra, J. Depauw, D. Gardès, P. Håkansson, Y. Le Beyec, A. Billebaud, M. Fallavier, J. Remillieux, J. C. Poizat, and J. P. Thomas, *Nucl. Instrum. Methods Phys. Res. B* **94**, 341 (1994).
- [5] C. Tomaschko, D. Brandl, R. Kugler, M. Schurr, and H. Voit, *Nucl. Instrum. Methods Phys. Res. B* **103**, 407 (1995).
- [6] A. Brunelle, S. Della-Negra, J. Depauw, D. Jacquet, Y. Le Beyec, M. Pautrat, and Ch. Schoppmann, *Nucl. Instrum. Methods Phys. Res. B* **125**, 207 (1997).
- [7] Y. Takahashi, T. Hattori, and N. Hayashizaki, *Phys. Rev. A* **75**, 013202 (2007).
- [8] D. Ben-Hamu, A. Baer, H. Feldman, J. Levin, O. Heber, Z. Amitay, Z. Vager, and D. Zajfman, *Phys. Rev. A* **56**, 4786 (1997).
- [9] K. Narumi, K. Nakajima, K. Kimura, M. Mannami, Y. Saitoh, S. Yamamoto, Y. Aoki, and H. Naramoto, *Nucl. Instrum. Methods Phys. Res. B* **135**, 77 (1998).
- [10] Y.-X. Shen, D.-X. Jiang, X.-T. Lu, and D.-Y. Shen, *Chin. Phys. Lett.* **18**, 525 (2001).
- [11] Y.-N. Wang and T.-C. Ma, *Phys. Lett. A* **178**, 209 (1993).
- [12] T. Takamoto and T. Kaneko, *Nucl. Instrum. Methods Phys. Res. B* **153**, 21 (1999).
- [13] S. Heredia-Avalos, R. Garcia-Molina, and I. Abril, *Nucl. Instrum. Methods Phys. Res. B* **164-165**, 296 (2000).
- [14] J. Jensen and P. Sigmund, *Phys. Rev. A* **61**, 032903 (2000).
- [15] S. Heredia-Avalos and R. Garcia-Molina, *Phys. Lett. A* **275**, 73 (2000).
- [16] R. Garcia-Molina and S. Heredia-Avalos, *Phys. Rev. A* **63**, 044901 (2001).
- [17] T. Kaneko, *Phys. Rev. A* **66**, 052901 (2002).
- [18] R. Garcia-Molina and M. D. Barriga-Carrasco, *Phys. Rev. A* **68**, 054901 (2003).
- [19] M. D. Barriga-Carrasco and R. Garcia-Molina, *Phys. Rev. A* **68**, 062902 (2003).
- [20] M. D. Barriga-Carrasco and R. Garcia-Molina, *Phys. Rev. A* **70**, 032901 (2004); S. Heredia-Avalos, I. Abril, C. D. Denton, and R. Garcia-Molina, *ibid.* **75**, 012901 (2007).
- [21] M. Vicanek, I. Abril, N. R. Arista, and A. Gras-Martí, *Phys. Rev. A* **46**, 5745 (1992).
- [22] E. Nardi and Z. Zinamon, *Phys. Rev. A* **51**, R3407 (1995).
- [23] F. J. Pérez-Pérez, I. Abril, R. Garcia-Molina, and N. R. Arista, *Phys. Rev. A* **54**, 4145 (1996).
- [24] F. J. Pérez-Pérez, I. Abril, N. R. Arista, and R. Garcia-Molina, *Nucl. Instrum. Methods Phys. Res. B* **115**, 18 (1996).
- [25] Z. L. Mišković, W.-K. Liu, and Y.-N. Wang, *Phys. Rev. A* **58**, 2191 (1998).
- [26] Y.-N. Wang, H.-T. Qiu, and Z. L. Mišković, *Phys. Rev. Lett.* **85**, 1448 (2000).
- [27] S. Heredia-Avalos, C. D. Denton, R. Garcia-Molina, and I. Abril, *Phys. Rev. Lett.* **88**, 079601 (2002).
- [28] E. Nardi, Z. Zinamon, T. A. Tombrello, and N. M. Tanushev, *Phys. Rev. A* **66**, 013201 (2002).
- [29] R. Garcia-Molina, I. Abril, C. D. Denton, and N. R. Arista, *Nucl. Instrum. Methods Phys. Res. B* **164-165**, 310 (2000).
- [30] R. Garcia-Molina, C. D. Denton, I. Abril, and N. R. Arista, *Phys. Rev. A* **62**, 012901 (2000).
- [31] J. Remillieux, *Nucl. Instrum. Methods* **170**, 31 (1980).
- [32] G. E. P. Box and M. E. Muller, *Ann. Math. Stat.* **29**, 610 (1958).
- [33] W. Brandt and M. Kitagawa, *Phys. Rev. B* **25**, 5631 (1982).
- [34] J. F. Ziegler, J. P. Biersak, and U. Littmark, *The Stopping and Ranges of Ions in Matter* (Plenum, New York, 1985), Vol. 1.
- [35] N. D. Mermin, *Phys. Rev. B* **1**, 2362 (1970).
- [36] I. Abril, R. Garcia-Molina, C. D. Denton, F. J. Pérez-Pérez, and N. R. Arista, *Phys. Rev. A* **58**, 357 (1998).
- [37] I. Abril, R. Garcia-Molina, N. R. Arista, and C. F. Sanz-Navarro, *Nucl. Instrum. Methods Phys. Res. B* **190**, 89 (2002); J. C. Moreno-Marín, I. Abril, and R. Garcia-Molina, *ibid.* **193**, 30 (2002).
- [38] S. Heredia-Avalos, J. C. Moreno-Marín, I. Abril, and R. Garcia-Molina, *Nucl. Instrum. Methods Phys. Res. B* **230**, 118 (2005).
- [39] S. Heredia-Avalos, R. Garcia-Molina, J. M. Fernández-Varea, and I. Abril, *Phys. Rev. A* **72**, 052902 (2005).
- [40] P. M. Echenique, R. H. Ritchie, and W. Brandt, *Phys. Rev. B* **20**, 2567 (1979).
- [41] L. Lammich, H. Buhr, H. Kreckel, S. Krohn, M. Lange, D. Schwalm, R. Wester, A. Wolf, D. Strasser, D. Zajfman, Z. Vager, I. Abril, S. Heredia-Avalos, and R. Garcia-Molina, *Phys. Rev. A* **69**, 062904 (2004).
- [42] *Handbook of Mathematical Functions*, edited by M. Abramowitz and I. A. Stegun (Dover, New York, 1972).
- [43] W. Möller, G. Pospiech, and G. Schrieder, *Nucl. Instrum. Methods* **130**, 265 (1975).
- [44] D. Zajfman, G. Both, E. P. Kanter, and Z. Vager, *Phys. Rev. A* **41**, 2482 (1990).
- [45] L. Meyer, *Phys. Status Solidi B* **44**, 253 (1971).
- [46] W. Williamson, Jr. and G. C. Duncan, *Am. J. Phys.* **54**, 262 (1986).
- [47] G. Schiwietz and P. L. Grande, *Nucl. Instrum. Methods Phys. Res. B* **175-177**, 125 (2001).
- [48] K. B. Winterbon, *Nucl. Instrum. Methods* **144**, 311 (1977).
- [49] Collection of stopping power data prepared by H. Paul, <http://www.exphys.uni-linz.ac.at/stopping/>.
- [50] M. J. Gaillard, J. C. Poizat, A. Ratkowski, J. Remillieux, and M. Auzas, *Phys. Rev. A* **16**, 2323 (1977).
- [51] M. J. Gaillard, J. C. Poizat, and J. Remillieux, *Phys. Rev. Lett.* **41**, 159 (1978).
- [52] N. Cue, N. V. de Castro-Faria, M. J. Gaillard, J. C. Poizat, J.

- Remillieux, D. S. Gemmell, and I. Plesser, *Phys. Rev. Lett.* **45**, 613 (1980).
- [53] D. Maor, P. J. Cooney, A. Faibis, E. P. Kanter, W. Koenig, and B. J. Zabransky, *Phys. Rev. A* **32**, 105 (1985).
- [54] M. F. Steuer and R. H. Ritchie, *Nucl. Instrum. Methods Phys. Res. B* **40/41**, 372 (1989).
- [55] A. Brunelle, S. Della-Negra, J. Depauw, D. Jacquet, Y. Le Beyec, and M. Pautrat, *Phys. Rev. A* **59**, 4456 (1999).
- [56] Z. L. Mišković, S. G. Davison, F. O. Goodman, W.-K. Liu, and Y.-N. Wang, *Phys. Rev. A* **61**, 062901 (2000).
- [57] S. Heredia-Avalos, R. Garcia-Molina, and N. R. Arista, *Europhys. Lett.* **54**, 729 (2001).
- [58] S. Heredia-Avalos and R. Garcia-Molina (unpublished).
- [59] J. D. Watts and R. J. Bartlett, *J. Chem. Phys.* **96**, 6073 (1992).
- [60] A. Fura, F. Tureček, and F. W. McLafferty, *Int. J. Mass. Spectrom.* **217**, 81 (2002).
- [61] G. Orlova and J. Goddard, *Chem. Phys. Lett.* **363**, 486 (2002).
- [62] J. Haubrich, M. Mühlhäuser, and S. D. Peyerimhoff, *Phys. Chem. Chem. Phys.* **4**, 2891 (2002).
- [63] J. Haubrich, M. Mühlhäuser, and S. D. Peyerimhoff, *J. Mol. Spectrosc.* **228**, 31 (2004).
- [64] A. Van Orden and R. J. Saykally, *Chem. Rev. (Washington, D.C.)* **98**, 2313 (1998).
- [65] J. K. Labanowski and I. Filippov, computational chemistry list at <http://server.ccl.net/>.
- [66] R. Garcia-Molina, I. Abril, C. D. Denton, and N. R. Arista, *Nucl. Instrum. Methods Phys. Res. B* **164-165**, 310 (2000).
- [67] R. Garcia-Molina, S. Heredia-Avalos, and I. Abril, *J. Phys.: Condens. Matter* **12**, 5519 (2000).
- [68] A. Faibis, E. P. Kanter, L. M. Tack, E. Bakke, and B. J. Zabransky, *J. Phys. Chem.* **91**, 6445 (1987).
- [69] A. Chiba, Y. Saitoh, and S. Tajima, *Nucl. Instrum. Methods Phys. Res. B* **232**, 32 (2005).